

Surface phase transitions at O and CO catalytic reaction on Pd(1 1 1)

E.E. Tornau^{a,*}, V. Petrauskas^a, G. Zvejnieks^{b,c}

^a Semiconductor Physics Institute, Goštauto 11, LT-01108, Vilnius, Lithuania

^b Department of Physics, University of Latvia, Raina 19, LV-1586, Riga, Latvia

^c Institute for Solid State Physics, Kengaraga 8, LV-1063, Riga, Latvia

Available online 27 April 2006

Abstract

The model has been proposed to simulate numerically the reaction $O + CO \rightarrow CO_2$ and occurring phase transitions on Pd(1 1 1) surface. We calculate the phase diagram for this system by kinetic Monte Carlo method. It shows the phase transitions $p(2 \times 2)_O \rightarrow \sqrt{3} \times \sqrt{3}R30^\circ$ and $p(2 \times 2)_O \rightarrow \sqrt{3} \times \sqrt{3}R30^\circ \rightarrow p(2 \times 1)_O$ with increase of CO coverage for room and intermediate temperatures, respectively, while in the low temperature limit the direct $p(2 \times 2)_O \rightarrow p(2 \times 1)_O$ phase transition is observed. We demonstrate that the reaction rate is the crucial factor determining the occurrence of the $p(2 \times 1)_O$ phase and vanishing of the $\sqrt{3} \times \sqrt{3}R30^\circ$ with decrease of temperature. The results indicate that the reaction proceeds inside both the $p(2 \times 2)_O$ and $\sqrt{3} \times \sqrt{3}R30^\circ$ phases, but on the perimeter of the domains of $p(2 \times 1)_O$ structure.

© 2006 Elsevier B.V. All rights reserved.

PACS: 68.43.Fg; 68.43.Hn; 68.43.Mn; 64.60.Cn

Keywords: CO oxidation; Catalytic reaction; Pd(1 1 1) surface; Kinetic Monte Carlo method; Phase transitions

1. Introduction

Catalytic reaction $O + CO \rightarrow CO_2$ on transition metal surfaces, and Pd(1 1 1) in particular, are intensively studied for almost 30 years (considering pioneering works [1,2]), but only during last decade improvement of STM and computing techniques led to real outburst of information on this subject. On one hand new studies are stimulated by a possibility to improve the technology of car exhaust catalytic converter. At the same time these studies raise fundamental questions regarding microscopic physico-chemical nature of reaction mechanisms and possible reaction paths, reasons of surface reactivity, conditions of CO oxidation, substrate–adsorbate interactions, etc.

As a substrate for catalytic CO oxidation, the Pd(1 1 1) has some distinguished features in comparison with other hexagonal closed-packed transition metal and metal oxide surfaces. The activation energy for the reaction on Pd(1 1 1) is quite high and, possibly, depends on CO coverage [1]. Mixed O–CO phases and on-top or bridge site positions of CO are

favoured on Pd(1 1 1) much less than, e.g., on a similar Pt(1 1 1) surface at least for small CO coverages. The unique feature of Pd(1 1 1) surface is the occurrence of high density oxygen $p(2 \times 1)_O$ structure under compression.

Oxidation of CO on Pd(1 1 1) proceeds simultaneously with the ordering of O and CO species. Thus, at room temperatures atomic oxygen O/Pd(1 1 1) prefers the ordered structure $p(2 \times 2)_O$. The $\sqrt{3} \times \sqrt{3}R30^\circ$ phase is obtained only under special conditions—additional uptake of oxygen at 270 K or its compression by add-on atoms [2,3]. For example, adsorbed CO on oxygen precovered Pd(1 1 1), easily compresses the $p(2 \times 2)_O$ oxygen structure into $\sqrt{3} \times \sqrt{3}R30^\circ$ and creates the place for its own domains [1–5]. However, the reaction is delayed till the occurrence of $\sqrt{3} \times \sqrt{3}R30^\circ$ phase [3], the fact which is quite unusual in comparison with other similar surfaces.

The vast majority of DFT calculations [4,6,7] as well as combined studies of both DFT and experimental data [2,3,8] support the viewpoint that oxygen reside on hollow three-fold fcc sites of Pd(1 1 1). An exception is the ion scattering study [9] which claims higher binding energy of the three-fold hcp sites. It should be noted that the difference in calculated binding energies of oxygen atoms on fcc and hcp sites is usually quite small.

* Corresponding author.

E-mail address: et@et.pfi.lt (E.E. Tornau).

The rest sites of CO on Pd(1 1 1) are well determined in the limit of small CO coverages. It is observed that CO molecules prefer the occupation of the fcc sites up to 0.5 ML of CO coverage [10–14]. Consequently they occupy the fcc sites in the $\sqrt{3} \times \sqrt{3}R30^\circ$ phase (0.33 ML CO coverage) which is a preferential phase for low CO coverages in CO/Pd(1 1 1) system. However, higher CO coverages allow several interpretations. Photoelectron diffraction study of Giessel et al. [10] shows that CO occupies both fcc and hcp sites forming the $c(4 \times 2)$ phase with CO coverage 0.5 ML. This is confirmed by the DFT calculations [11]. This calculation predicts also the top site occupation for phases with high CO coverage (0.75 ML). STM study [14] suggests the alternative explanation for $c(4 \times 2)$ phase: CO either occupies both fcc and hcp sites or forms this phase on bridge sites.

The possible reaction paths are estimated using the DFT calculations by Salo et al. [6]. They convincingly demonstrate that nearest neighbor (NN) fcc sites for O and CO, the so-called fcc–fcc (horizontal) location, is the most probable initial position for reaction.

Thus it might be summarized that O and CO adsorbed on Pd(1 1 1) diffuse mostly over fcc sites when forming their ordered structures. The type of ordered structure and sequence of phase transitions depend on temperature, and three different temperature regimes can be distinguished experimentally. At room temperature the initial $p(2 \times 2)_O$ phase is compressed into $\sqrt{3} \times \sqrt{3}R30^\circ$ with increase of CO coverage. At intermediate temperature there is a sequence of two phase transitions with increasing CO coverage: $p(2 \times 2)_O \rightarrow \sqrt{3} \times \sqrt{3}R30^\circ \rightarrow p(2 \times 1)_O$ (or $p(2 \times 1)_{O+CO}$). At low temperature, when oxygen atoms are almost immobile and diffusion of CO molecules and reaction are very slow, intermediate $\sqrt{3} \times \sqrt{3}R30^\circ$ phase is unobservable [3].

Here we perform the kinetic Monte Carlo (MC) simulations of CO oxidation and catalytic reaction on Pd(1 1 1) in temperature range between 160 and 300 K. Our aim is to study occurring phase transitions and their sequences, growth of different domains and reaction rate dependence on pressure and temperature. The O and CO system on Pd(1 1 1) is challenging for kinetic MC modeling. First, because of strong NN repulsive interactions between the ordering species. For example, the fact that $p(2 \times 1)_O$ phase occurs only under compression confirms the presence of a strong repulsion between NN O atoms. The preference of $\sqrt{3} \times \sqrt{3}R30^\circ$ phase in pure CO/Pd(1 1 1) indicates the CO–CO repulsion at least between the molecules at the NN sites. The shapes of domains of phases in O and CO on Pd(1 1 1) system evidence that there is a strong repulsion between O and CO components. Therefore, the reaction proceeds on highly repulsive sites which is the probable reason of delay of reaction onset. Actually such modelling, especially seeking semi-quantitative comparison with the experiment, is quite rare (see, e.g. [15]).

Second, the experiments [3] have been performed for considerable temperature range. Since both diffusion and reaction rates are taken in the activated form they experience drastic changes with temperature. Thus, it is a way to link the

data obtained in both STM experiments and DFT calculations (rest sites, values of activation energies, pre-exponential factors and interaction constants) used as an input in our MC simulation to the results obtained in the output—types of phases and domains and possible phase transitions.

Third, MC simulations allow us to estimate the most probable reaction sites location—inside the oxygen domains or along the perimeter of O and CO structures. Such a problem was studied recently by combined STM and MC simulations for O and CO system on Pt(1 1 1) [16].

2. Model

We assume that the Langmuir–Hishelwood type reaction proceeds between chemisorbed oxygen atoms and CO molecules on the hexagonal lattice (with periodic boundary conditions) composed of the fcc sites of Pd(1 1 1). As an initial phase we use ordered $p(2 \times 2)_O$ structure. The processes considered are CO adsorption, O and CO diffusion (hopping) over the NN fcc sites, and $O + CO \rightarrow CO_2$ reaction for O and CO atoms residing in the NN sites only. We assume that the desorption of CO is negligible due to very high activation barrier for desorption [17], while CO_2 is desorbed from the surface immediately upon formation [1,6].

2.1. The choice of interaction parameters

These parameters describe O–O, CO–CO and O–CO interactions and have to be chosen to satisfy the following requirements: reproduction of three ordered oxygen phases, preference of CO to build up their own $\sqrt{3} \times \sqrt{3}R30^\circ$ structure, and strong mutual repulsion of O and CO species observed in experiments [3,5].

To obtain the $p(2 \times 2)_O$ structure, the set of interaction parameters between NN (lattice constant a), next-NN ($\sqrt{3}a$) and 3-rd NN ($2a$) oxygen atoms have to be accounted for. Due to the lack of data from experiments or first principles calculations, as a first approximation we have chosen a simplified set of oxygen interaction constants proposed earlier for the $p(2 \times 2)_O$ phase in a similar O/Ru(0 0 1) system [18]: $v_1^O = 0.16$ eV, $v_2^O = 0.1v_1^O$ and $v_3^O = -0.01v_1^O$. Strong repulsion of NN and very weak attraction of the third are sufficient factors to stabilize the $p(2 \times 2)_O$ structure.

For interaction between CO molecules we have chosen the set recently proposed from STM measurements of CO/Pd(1 1 1) at low CO coverage c_{CO} [13]: $v_1^{CO} = 0.04$ eV, $v_2^{CO} = -0.001$ eV and $v_3^{CO} = 0.01$ eV. This set favors the formation of the $\sqrt{3} \times \sqrt{3}R30^\circ_{CO}$ structure, and, being of much weaker repulsion than that taken for O–O and O–CO interaction gives way for relative attraction inside the CO domains. We considered only NN repulsive O–CO interaction, $v_1^{O-CO} = v_1^O = 0.16$ eV.

2.2. The choice of kinetic parameters

Hopping rates of O and CO were taken in the activated form $v_X = v_0^X \exp(-E_a^X/k_B T)$, where k_B is Boltzmann constant, T —

temperature and index X denotes either O or CO. The reaction rate was $v_r = v_0^r \exp(-E_a^r/k_B T)$. Parameters characterizing the hopping of oxygen were activation energy $E_a^O = 0.4$ eV (which is the lower limit of that obtained by the STM measurements [8] and rather close to E_a^O on Pt(1 1 1) [19]) and pre-exponential factor $v_0^O = 10^{12} \text{ s}^{-1}$ [8]. The value for hopping of CO, $E_a^{\text{CO}} = 0.12$ eV, was chosen in accordance with the STM result [13], but the pre-exponential factor $v_0^{\text{CO}} = 10^8 \text{ s}^{-1}$ was four orders of magnitude lower than the experimental. This choice allows to perform the simulation in a real time scale and fulfills the requirement $v_{\text{CO}} \gg v_O$.

From molecular beam experiments in high and moderate CO coverage limit the activation energy E_a^r for the reaction was estimated as 0.6 eV [1,20] and pre-exponential factor as $10^{7 \pm 1} \text{ s}^{-1}$ [20]. In our simulations we took $E_a^r = 0.5$ eV, as suggested for the same reaction on Pt(1 1 1) [16], and varied v_0^r as a fit parameter. The variation yields $v_0^r = 10^9 \text{ s}^{-1}$ from the reaction delay condition at 300 K [3]. These values of reaction parameters allowed us both to obtain the delay and at the same time to perform the calculations in a sufficiently broad interval of temperature values 160–300 K. It should be also noted that the estimation $E_a^r = 0.6$ eV [1,20] was obtained combining experimental data with a simple second order kinetic mean field equations. The results of our simulations as well as other experiments (see, e.g. [3,5]), evidencing the occurrence of different domains, demonstrate the importance of correlation effects between chemisorbed O and CO species. It is well known from the phase transition theory that the mean field approach fails in the systems where correlations are strong and/or interactions strongly competing.

The CO adsorption flow was taken as pressure, p , and temperature dependent and calculated from the formulae $F = p/\sqrt{2\pi m T}$, where m stands for the mass of CO molecule. Main kinetic and interaction parameters are summarized in the Table 1.

In kinetic MC simulations we use the standard model dynamics described in Refs. [21,22]. Since the model contains bimolecular steps, e.g., diffusion and reaction, we exploit the *pair algorithm* [21]. The basic idea of the algorithm is to consider *two* NN sites simultaneously and account for all

possible processes therein. Kinetic MC simulations contain the following steps:

- (1) The time update is determined in the following way. Firstly, from the pair configurations:

$$\square-\square : \text{adsorption in } \square + \text{adsorption in } \square \quad q_1 = 2F, \quad (1)$$

$$\text{CO}-\square : \text{hopping of CO} + \text{adsorption in } \square \quad q_2 = 2v_{\text{CO}} + F, \quad (2)$$

$$\text{O}-\square : \text{hopping of O} + \text{adsorption in } \square \quad q_3 = 2v_O + F, \quad (3)$$

$$\text{CO}-\text{O} : \text{reaction} \quad q_4 = v_r, \quad (4)$$

the parameter τ is determined as $\tau = 1/\max(q_i)$ (\square denotes vacancy in Eqs. (1)–(3)). In the considered model τ is determined by the step containing diffusion of CO, which is the fastest process in the model, i.e., $\tau = 1/q_2$. Further in MC simulations we use the rates normalized to unity. They are obtained by multiplication with τ . Finally, the simulation time update in the pair algorithm is found as $\Delta t = 2\tau/L^2$.

Multiplication of both hopping rates v_{CO} and v_O by a factor of two in Eqs. (2) and (3) arises from the requirement $\Delta t = \text{constant}$ in the pair algorithm and possibility to estimate maximal values of the energetic interactions between species in the standard model [21]. The hopping steps require additional calculation and will be explained in the step (4).

- (2) Simulation time is updated, $t \rightarrow t + \Delta t$.
- (3) The pair of neighboring sites is chosen randomly on a hexagonal lattice.
- (4) According to the configuration of the pair, one of independent processes listed in the second column of Eqs. (1)–(4) is started with the corresponding weight. As an example, let us consider a pair in the state CO– \square , Eq. (2). The hopping step of CO is started when a generated random number (RN) is less than $2v_{\text{CO}}\tau$, while the adsorption step is completed if $2v_{\text{CO}}\tau < \text{RN} < q_2\tau$.

Table 1

Process	Schematic definition	Formulae	Parameters used in simulation
Adsorption	$\text{CO (gas)} + \square \rightarrow \text{CO (ads)}$	CO flow $F = p/\sqrt{2\pi m T}$	$p = (0.5\text{--}5) \times 10^{-7} \text{ Torr}$ [3]
Reaction	$\text{CO (ads)} + \text{O (ads)} \rightarrow \text{CO}_2 \rightarrow \square + \square$	$v_r = v_0^r \exp(-E_a^r/k_B T)$	$E_a^r = 0.5 \text{ eV}$, $v_0^r = 10^9 \text{ s}^{-1}$ (fit)
Diffusion	$\text{O} + \square \rightarrow \square + \text{O}$	$v_{\text{O}}^{\text{int}} = \frac{2v_0^{\text{O}} \exp(-E_a^{\text{O}}/k_B T)}{1 + \exp((E_\beta^{\text{O}} - E_\alpha^{\text{O}})/k_B T)}$	$E_a^{\text{O}} = 0.4 \text{ eV}$ [8], $v_0^{\text{O}} = 10^{12} \text{ s}^{-1}$ [8]
	$\text{CO} + \square \rightarrow \square + \text{CO}$	$v_{\text{CO}}^{\text{int}} = \frac{2v_0^{\text{CO}} \exp(-E_a^{\text{CO}}/k_B T)}{1 + \exp((E_\beta^{\text{CO}} - E_\alpha^{\text{CO}})/k_B T)}$	$E_a^{\text{CO}} = 0.12 \text{ eV}$ [13], $v_0^{\text{CO}} = 10^8 \text{ s}^{-1}$
Interaction (fcc sites)	NN, NNN and 3NN for O–O and CO–CO, NN for O–CO	$E_{\alpha,\beta}^{\text{O}} = \sum_{i=1}^3 v_i^{\text{O}} n_i^{\text{O}} + v_1^{\text{O-CO}} n_1^{\text{O-CO}}$	$v_1^{\text{O}} = 0.16 \text{ eV}$ [18], $v_2^{\text{O}} = 16 \text{ meV}$ [18], $v_3^{\text{O}} = -1.6 \text{ meV}$ [18]
		$E_{\alpha,\beta}^{\text{CO}} = \sum_{i=1}^3 v_i^{\text{CO}} n_i^{\text{CO}} + v_1^{\text{O-CO}} n_1^{\text{O-CO}}$	$v_1^{\text{CO}} = 0.04 \text{ eV}$ [13], $v_2^{\text{CO}} = -1 \text{ meV}$ [13], $v_3^{\text{CO}} = 10 \text{ meV}$ [13] $v_1^{\text{O-CO}} = 0.16 \text{ eV}$ [13]

Adsorption and reaction steps are completed instantly, while the hopping step of both O and CO requires additional accounting for the change of configuration. A parameter $\Delta\omega = (E_{\beta}^X - E_{\alpha}^X)/k_B T$ describing energy difference between final β and initial α states is calculated. The energy of the state is given by $E_{\alpha,\beta}^X = \sum_{i=1}^3 v_i^X n_i^X + v_1^{O-CO} n_1^{O-CO}$, where n_i^X is the number of neighbors up to the third of the same sort as initial atom and n_1^{O-CO} is number of NN of the different sort. When a newly generated RN fulfills the condition $RN < 1/[1 + \exp(\Delta\omega)]$ the hopping step is completed, otherwise the configuration stays unchanged. Thus, the real hopping rate of interacting species reads as $v_X^{int} = 2v_X/(1 + \exp(\Delta\omega))$. Moreover, in the limit of noninteracting species ($\Delta\omega = 0$) hopping occurs in the half of considered cases (when $RN < 1/2$) which effectively cancel the multiplication by two in Eqs. (2) and (3) leading to hopping rates v_{CO} and v_O , respectively.

- (5) The program returns to step (2) if time t is less than the final simulation time.

3. Results and discussions

We performed simulations on hexagonal lattices of sizes 48×48 , 72×72 and 96×96 Pd atoms. In order to reduce the finite size effects, the lattice size was varied to keep the largest simulated structure sizes $\ll L$, where L is the lattice side length in the units of lattice constant. Exceptions were the cases of both global phases $p(2 \times 2)_O$ and $\sqrt{3} \times \sqrt{3}R30^\circ_0$ that occur on whole lattice by definition. We start the simulation from the ordered structure $p(2 \times 2)_O$ obtained by annealing of $c_O = 0.25$ oxygen atoms at $T = 230$ K, where c_O is concentration of oxygen atoms. Upon adsorption of CO the characteristic features of reaction and phase transitions allow us to distinguish three qualitatively different temperature ranges: (i) high temperature range (around 300 K), where $p(2 \times 2)_O \rightarrow \sqrt{3} \times \sqrt{3}R30^\circ_0$ phase transition is obtained, (ii) intermediate temperature range ($185 < T < 285$ K), where the sequence of $p(2 \times 2)_O \rightarrow \sqrt{3} \times \sqrt{3}R30^\circ_0 \rightarrow p(2 \times 1)_O$ phase transitions is obtained and (iii) low temperature range ($T < 185$ K) where the transition $p(2 \times 2)_O \rightarrow p(2 \times 1)_O$ is obtained. It should be noted that reaction which is quite fast at 300 K is almost negligible at 230 K. The reaction delay is seen as constant c_O at the initial stage of the $T = 300$ K curve and it is present at lower temperature values as well (see Fig. 1).

All our calculations are performed for fixed pressure value 2×10^{-7} Torr except for Fig. 2, where time dependence of the reaction product is studied for different values of pressure. The decrease of CO pressure restricts the adsorption rate, which in turn prolongs the survival probability of oxygen atoms in time. This is reflected as a decrease as well as a shift of the maximum of CO_2 production in time, the result which qualitatively agrees with mass spectrometry data by Mendez et al. [3].

Along with the temporal monitoring of the simulated snapshots, pair correlation functions (CF) have been introduced to analyze the ordered spatial structures. We define CF as $\eta^{O-O}(r) = c_{OO}(r)/c_O^2$, where $c_{OO}(r)$ is concentration of O–O pairs at a distance r . It should be noted, that in the mean field

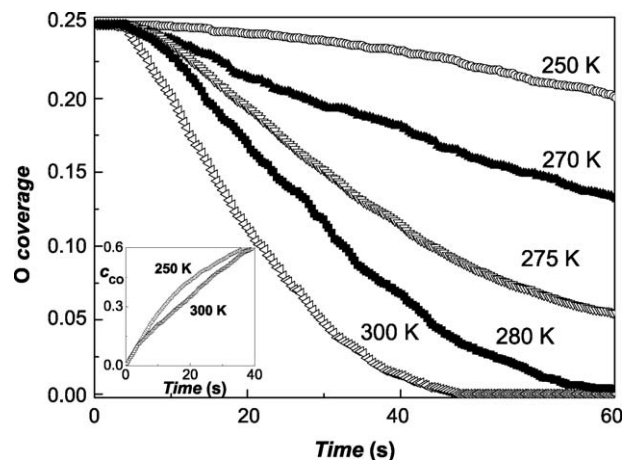


Fig. 1. Time dependence of oxygen and CO (inset) coverage for different temperature values, $p = 2 \times 10^{-7}$ Torr.

limit $c_{OO}(r) = c_O^2$, which leads to $\eta^{O-O}(r) = 1$. The condition $\eta^{O-O}(r_c) = 1$ allows us to estimate the oxygen domain radius r_c . In order to describe oxygen spatial structures, we consider two radial directions regarding the initial atom: (a) NN direction with the distance between atoms given by $r = ka$ and (b) NNN direction with $r = k\sqrt{3}a$. The index $k = 1, 2, \dots$, is subject to restraint $r/a \leq L/2$. To obtain the full spatial information in the same way we calculate the CF $\eta^{CO-CO}(r)$ and $\eta^{O-CO}(r)$.

We introduce order parameters $\eta_{2 \times 1} = 3\eta^{O-O}(a)c_O$, $\eta_{\sqrt{3} \times \sqrt{3}} = \eta^{O-O}(a\sqrt{3})c_O$ and $\eta_{2 \times 2} = \eta^{O-O}(2a)c_O$ as a measure for occurring oxygen structures and corresponding phase transitions. They are normalized in such a way that the parameter of the certain ideal phase is equal to unity, while the remaining two parameters are zero except the case of the $p(2 \times 1)_O$ phase when $\eta_{2 \times 1} = 1$, but $\eta_{2 \times 2}$ and $\eta_{\sqrt{3} \times \sqrt{3}}$ are nonzero. The phase transition point is determined as the crossing point of these parameters.

The characteristic order parameters for three different temperature limits are presented in Fig. 3. In the high temperature limit (see Fig. 3(a)) the $p(2 \times 1)_O$ structure is

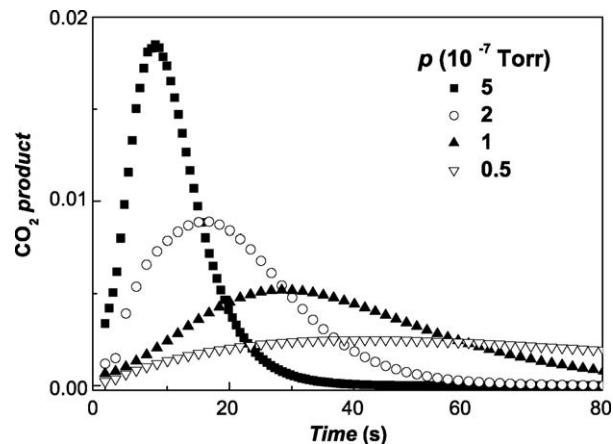


Fig. 2. Time dependence of CO_2 product for $T = 300$ K and different values of pressure, $p = 5 \times 10^{-7}$ (squares), 2×10^{-7} (circles), 1×10^{-7} (up-triangles), 0.5×10^{-7} (down-triangles) Torr.

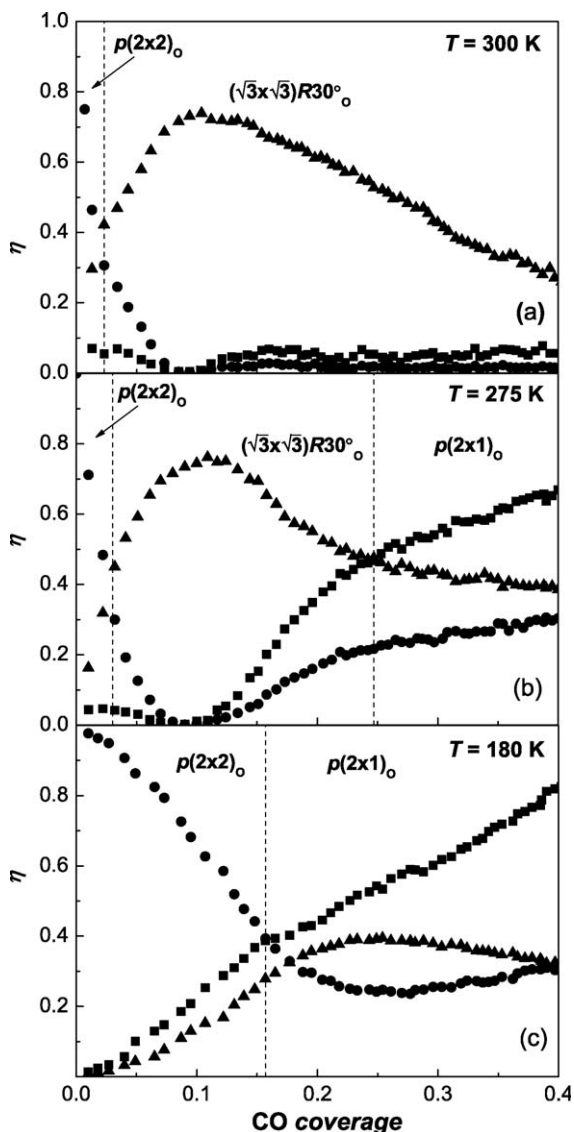


Fig. 3. Order parameter $\eta_{2 \times 1}$ (squares), $\eta_{\sqrt{3} \times \sqrt{3}}$ (triangles) and $\eta_{2 \times 2}$ (circles) dependence on CO coverage in three different temperature limits, $T = 300$ K (a), 275 K (b), 180 K (c). Vertical dotted lines mark phase transitions.

unreachable, and just a single transition $p(2 \times 2)_O \rightarrow \sqrt{3} \times \sqrt{3}R30^\circ$ takes place at small CO coverage (< 0.03). The order parameters show very abrupt behavior similar to that of the first order phase transition. All this indicates that initial $p(2 \times 2)_O$ structure is very unstable against CO compression and the difference of free energies of both phases is very small in this temperature range, the finding strongly supporting the results obtained by the DFT calculation [4].

The kinetics of $p(2 \times 2)_O \rightarrow \sqrt{3} \times \sqrt{3}R30^\circ$ transition at temperature $T = 300$ K is the following. The vacant sites are occupied by adsorbed highly mobile CO molecules which compress the initial $p(2 \times 2)_O$ structure leading to $\sqrt{3} \times \sqrt{3}R30^\circ$ reconstruction. At $t = 2.7$ s the $\sqrt{3} \times \sqrt{3}R30^\circ$ phase is stoichiometric and composed of $c_O = 0.25$ and $c_{CO} = 0.08$. The reaction starts with delay at $t = 4$ s. With further increase of CO, when total coverage $c = c_O + c_{CO}$ exceeds the stoichiometry of this structure 0.33, the formation of separate CO

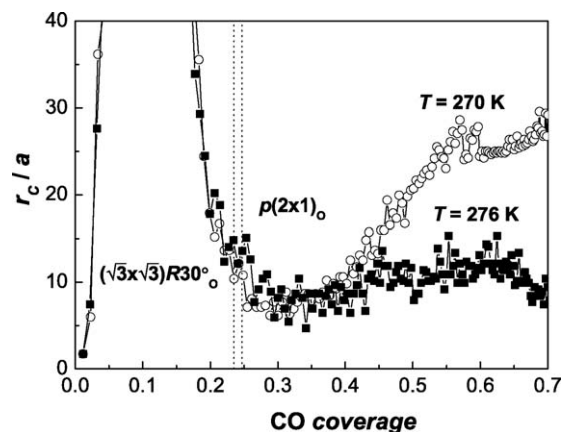


Fig. 4. Oxygen domain radius dependence on CO coverage obtained from correlation function $\eta^{0-O}(ka\sqrt{3})$ analysis at $T = 270$ and 276 K. Two dashed vertical lines indicate phase transition between $\sqrt{3} \times \sqrt{3}R30^\circ$ and $p(2 \times 1)_O$ phases at both these temperature values, respectively.

domains starts. The CO domains are more compressed than $\sqrt{3} \times \sqrt{3}R30^\circ$ domains due to chosen condition $v_1^0 = v_1^{0-CO} > v_1^{CO}$, and only up to $c_{CO} \sim 0.1$ show the rudiments of the $\sqrt{3} \times \sqrt{3}R30^\circ$ structures, which never are formed into larger structure of this symmetry. In what follows ($c_{CO} = 0.09-0.2$) the CO molecules are accumulated into denser islands. The $p(2 \times 1)_O$ phase is absent since the reaction proceeds quite fast, and in the long-time limit, when total concentration reaches the stoichiometry of the phase $c \sim 0.5$, there are no oxygen atoms left to form the $p(2 \times 1)_O$ phase.

For intermediate temperatures below 290 K we find the sequence of phase transitions $p(2 \times 2)_O \rightarrow \sqrt{3} \times \sqrt{3}R30^\circ \rightarrow p(2 \times 1)_O$. At $T = 275$ K the initial $p(2 \times 2)_O$ phase is more stable than at higher temperature, i.e., more CO molecules are needed to induce the first transition to the $\sqrt{3} \times \sqrt{3}R30^\circ$ phase (see Fig. 3(b)). At $c_{CO} = 0.24$ the second transition takes place to denser $p(2 \times 1)_O$ phase. In this phase the correlation length

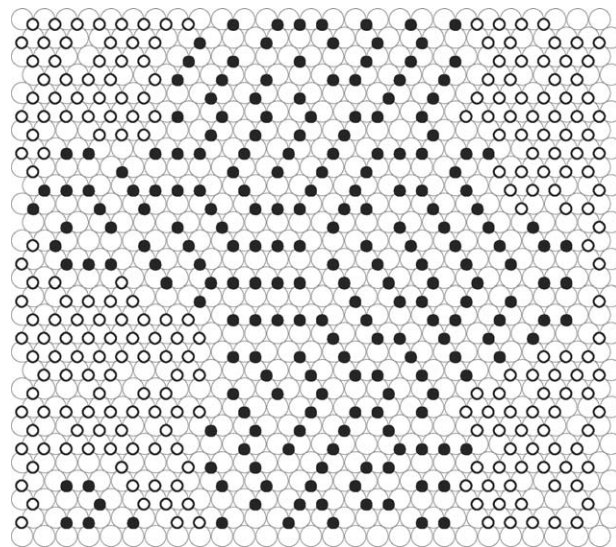


Fig. 5. The snapshot of one $p(2 \times 1)_O$ phase domain at $T = 275$ K and $c_{CO} = 0.56$. Oxygen atoms and CO molecules are denoted as solid and open circles, respectively.

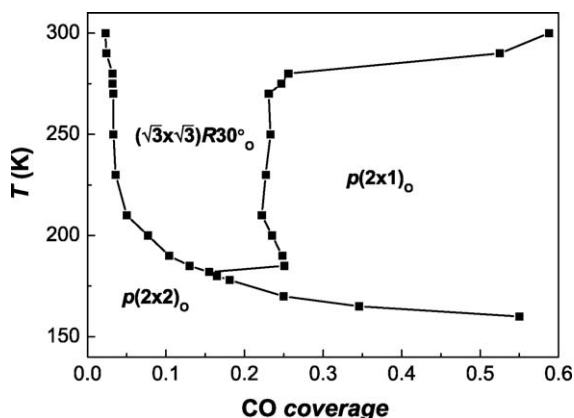


Fig. 6. Phase diagram with obtained oxygen structures.

for O atoms is finite contrary to the $\sqrt{3} \times \sqrt{3}R30^\circ$ phase. The $p(2 \times 1)_O$ phase occurs in compact domains of finite length.

In Fig. 4 the calculated domain radius is shown for two rather close values of temperature corresponding, however, to different reaction regimes. The curve for $T=276$ K is noteworthy for rather fast reaction regime causing occurrence of many small $p(2 \times 1)_O$ domains diminishing with increase of CO coverage. The curve for $T=270$ K represents much slower reaction and therefore growth of a few large $p(2 \times 1)_O$ domains. Our calculation indicates that crossover between these two regimes for chosen parameters of the model is around 275 K. Thus, the characteristic feature of temperature range $250 \text{ K} < T < 275 \text{ K}$ and concentrations $c = c_O + c_{CO} > 0.5$ is the accumulation of small $p(2 \times 1)_O$ domains into large clusters. The $p(2 \times 1)_O$ phase might grow in three directions on a hexagonal lattice, therefore the overall structure of a large domain is usually formed of all three bend 2×1 units as shown in the snapshot of Fig. 5.

At temperature below 200 K the mobility of oxygen atoms decreases so much that the $p(2 \times 2)_O$ phase is present up to CO coverage $\gtrsim 0.1$. The adsorption is even more promoted due to chosen condition for CO flow $F \sim 1/\sqrt{T}$, but reaction is very

weak. The interval of CO coverage, where the $\sqrt{3} \times \sqrt{3}R30^\circ$ phase exists, shrinks with decrease of temperature. At $T < 185$ K the system reaches the total coverage $c = 0.5$ necessary for $p(2 \times 1)_O$ phase formation rather fast and builds it directly bypassing the $\sqrt{3} \times \sqrt{3}R30^\circ$ phase (see Fig. 3(c)). Calculation of order parameters allows us to summarize the observed phase transitions in the phase diagram of Fig. 6. The triple point of all three phases coexistence is found at approximately 185 K.

Performed CF analysis allows us to estimate the spatial location of reaction sites, i.e., it answers to the question where the O–CO reaction most probably takes place – inside the loose oxygen-formed phases or along the perimeter of O and CO domains. It should be noted that in the global $p(2 \times 2)_O$ and $\sqrt{3} \times \sqrt{3}R30^\circ$ phases reaction proceeds on all distances since there are no O domain borders by definition. Oxygen clusters start to emerge after the $\sqrt{3} \times \sqrt{3}R30^\circ$ phase bypass its maximum and starts to shrink giving a way to rising $p(2 \times 1)_O$ phase domains with increase of CO coverage. Calculated CF $\eta^{O-CO}(r)$ demonstrate two qualitatively different types of behavior before and after the $\sqrt{3} \times \sqrt{3}R30^\circ \rightarrow p(2 \times 1)_O$ phase transition.

In the less compact $\sqrt{3} \times \sqrt{3}R30^\circ$ phase the CF $\eta^{O-CO}(r)$ shows two branches in Fig. 7(a). There is a large probability to find the O–CO pair in $\sqrt{3} \times \sqrt{3}R30^\circ$ structure, since $\eta^{O-CO}(r) > 1$ at distances corresponding to this structure, $r = k3a$ and $k\sqrt{3}a$ ($r < 25a$) (see upper branch of O–CO CF in Fig. 7(a)). Similarly the upper branch of O–O CF allow us to find the radius of oxygen $\sqrt{3} \times \sqrt{3}R30^\circ$ structure, $r_c = 25a$, where CF reach unity. Thus, it follows that there is a large probability to find O–CO pair within the cluster of O in the $\sqrt{3} \times \sqrt{3}R30^\circ$ structure. This implies that the reaction between O and CO proceeds inside oxygen clusters.

The lower branch of O–CO CF (Fig. 7(a)) is composed of values at distances $r = ka$ (excluding $r = 3ka$ points which characterize both $p(2 \times 1)_O$ and $\sqrt{3} \times \sqrt{3}R30^\circ$ structures). These correlations correspond to $p(2 \times 1)_O$ phase and indicate a reduced probability to find an O–CO pair in this structure. It is

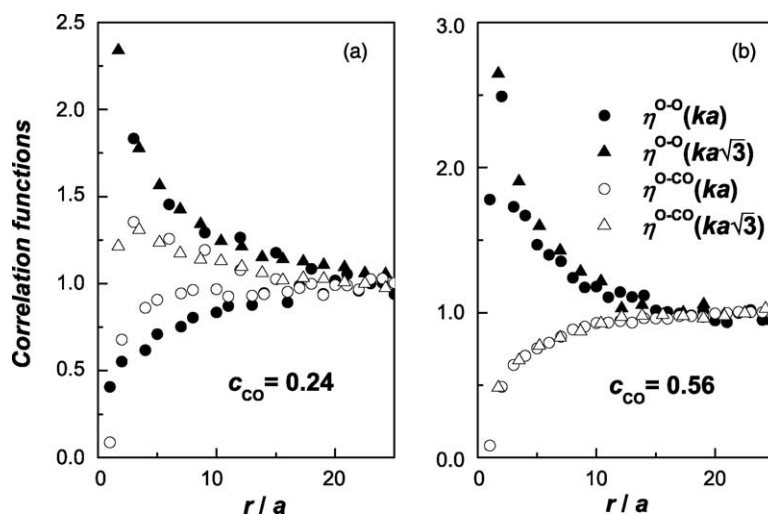


Fig. 7. Correlation functions $\eta^{O-O}(ka)$ (solid dots), $\eta^{O-O}(ka\sqrt{3})$ (solid triangles) and $\eta^{O-CO}(ka)$ (open dots) and $\eta^{O-CO}(ka\sqrt{3})$ (open triangles) for CO coverages c_{CO} : 0.24 (a) and 0.56 (b) at $T = 275$ K.

interesting to note, that we can observe smaller probability to find O–CO pair into O cluster even in the early stage of $p(2 \times 1)_O$ phase formation. The typical CF of $p(2 \times 1)_O$ phase are shown in Fig. 7(b). The domain size of the $p(2 \times 1)_O$ structure is $r_c = 15a$ at $c_{CO} = 0.56$. Within this distance there is a high probability to find the O–CO pair closer to the border of oxygen cluster, which implies that the reaction proceeds mostly on the boundary of the $p(2 \times 1)_O$ domain. The effective melting of oxygen clusters due to reaction on perimeter is confirmed in Fig. 4 by slow decrease of r_c with increase of CO coverage at high values of c_{CO} .

4. Conclusions

We present a kinetic MC simulation of phase transitions and catalytic $O + CO \rightarrow CO_2$ reaction on highly repulsive sites of Pd(1 1 1) surface. As input parameters our calculation uses both DFT and experimental data for interaction constants, hopping and reaction rates. However, two modifications to the input parameters were made. First, the pre-exponential factor for reaction was found as a fit parameter from the experimentally observed reaction delay condition at $T = 300$ K. Second, in order to perform our simulations in a realistic time scale, the pre-exponent for the hopping rate of CO was chosen four orders of magnitude lower than the experimental one. This approximation still fulfills the condition that the hopping rate of CO is the fastest process in the system and leads to a model, which qualitatively reproduces experimental observations. Therefore, we expect that increase of CO hopping rate to its experimental value will have no qualitative effects.

The considered temperature range is 160–300 K. Within the model we reproduce three qualitatively different temperature regimes observed experimentally [3]. In the high temperature limit we obtain a single phase transition $p(2 \times 2)_O \rightarrow \sqrt{3} \times \sqrt{3}R30^\circ$ with increase of CO concentration. This transition occurs almost instantly after the start of CO adsorption. The denser $p(2 \times 1)_O$ phase is absent due to high reaction rate which leaves no oxygen atoms to form this phase.

At intermediate values of temperature two phase transitions are observed $p(2 \times 2)_O \rightarrow \sqrt{3} \times \sqrt{3}R30^\circ \rightarrow p(2 \times 1)_O$. Contrary to the high temperature limit the second phase transition takes place due to slower reaction rate. There are sufficient oxygen atoms left which could be compressed to the $p(2 \times 1)_O$ phase.

The low temperature limit is characterized by direct $p(2 \times 2)_O \rightarrow p(2 \times 1)_O$ phase transition. The absence of the $\sqrt{3} \times \sqrt{3}R30^\circ$ phase can be explained by low mobility of the oxygen atoms. The time of the $\sqrt{3} \times \sqrt{3}R30^\circ$ phase occurrence is longer than the time required for the total concentration of reactants to exceed 0.5, the stoichiometry of the $p(2 \times 1)_O$ phase.

Since each temperature range demonstrates specific sequence of adsorbate structural transitions, we introduced

order parameters of the obtained phases and calculated the overall phase diagram. This diagram is qualitatively comparable with the tentative phase diagram obtained on a basis of the STM measurements [3].

Performed analysis of correlation functions allows us to predict the most probable locations for the $O + CO$ reaction. It turns out that in more loose $p(2 \times 2)_O$ and $\sqrt{3} \times \sqrt{3}R30^\circ$ phases the reaction proceeds inside oxygen phase and within oxygen clusters upon their formation. Contrary, in more compact $p(2 \times 1)_O$ structure the reaction takes place on the boundary between oxygen and CO domains.

Summarizing, the proposed model links the microscopic properties to the macroscopically observed spatio-temporal patterns. It provides the kinetic interpretation for phase transitions and predicts the reaction order.

Acknowledgements

We express our gratitude to V.N. Kuzovkov and S. Lapinskas for a number of fruitful discussions. We also thank Lithuanian State Studies and Science Foundation, EC project PRAMA and The European Social Fund for financial support.

References

- [1] T. Engel, G. Ertl, *J. Chem. Phys.* 69 (1978) 1267.
- [2] H. Conrad, G. Ertl, *J. Kippers*, *Surf. Sci.* 76 (1978) 323.
- [3] J. Mendez, S.H. Kim, J. Cerda, J. Winterlin, G. Ertl, *Phys. Rev. B* 71 (2005) 085409.
- [4] A.P. Seitsonen, Y.D. Kim, S. Schwegmann, H. Over, *Surf. Sci.* 468 (2000) 176.
- [5] T. Matsushita, H. Asada, *J. Chem. Phys.* 65 (1986) 1658.
- [6] P. Salo, K. Honkala, M. Alatalo, K. Laasonen, *Surf. Sci.* 516 (2002) 247.
- [7] C.J. Zhang, P. Hu, *J. Am. Chem. Soc.* 123 (2001) 1166.
- [8] M.K. Rose, A. Borg, J.C. Dunphy, T. Mitsui, D.F. Ogletree, M. Salmeron, *Surf. Sci.* 561 (2004) 69.
- [9] A. Steltenpohl, N. Memmel, *Surf. Sci.* 443 (1999) 13.
- [10] T. Giessel, O. Schaff, C.J. Hirshmuyl, V. Fernandez, K.-M. Schindler, A. Theobald, S. Bao, R. Lindsay, W. Berndt, A.M. Bradshaw, C. Baddeley, A.F. Lee, R.M. Lambert, D.P. Woodruff, *Surf. Sci.* 406 (1998) 90.
- [11] D. Loffreda, D. Simon, P. Sautet, *Surf. Sci.* 425 (1999) 68.
- [12] P. Sautet, M.K. Rose, J.C. Dunphy, S. Behler, M. Salmeron, *Surf. Sci.* 453 (2000) 25.
- [13] T. Mitsui, M.K. Rose, E. Fomin, D.F. Ogletree, M. Salmeron, *Phys. Rev. Lett.* 94 (2005) 036101.
- [14] M.K. Rose, T. Mitsui, J.C. Dunphy, A. Borg, D.F. Ogletree, M. Salmeron, P. Sautet, *Surf. Sci.* 512 (2002) 48.
- [15] V.P. Zhdanov, *Phys. Rev. Lett.* 77 (1996) 2109.
- [16] S. Völkening, J. Winterlin, *J. Chem. Phys.* 114 (2001) 6382.
- [17] X. Guo, J.T. Yates Jr., *J. Chem. Phys.* 90 (1989) 6761.
- [18] C. Stampfl, H.J. Kreuzer, S.H. Payne, H. Pfürer, M. Scheffler, *Phys. Rev. Lett.* 83 (1999) 2993.
- [19] J. Winterlin, *Adv. Catal.* 45 (2000) 131.
- [20] J. Libuda, I. Meusel, J. Hoffmann, J. Hartmann, L. Piccolo, C.R. Henry, H.-J. Freund, *J. Chem. Phys.* 114 (2001) 4669.
- [21] G. Zvejnicks, V.N. Kuzovkov, *Phys. Rev. E* 63 (2001) 051104.
- [22] V.N. Kuzovkov, E.A. Kotomin, G. Zvejnicks, *Comput. Modell. New Technol.* 8 (2004) 7.